Geophysical Research Letters

RESEARCH LETTER
10.1029/2020GL091596

Pluto's Antipodal Terrains Imply a Thick Subsurface Ocean and Hydrated Core

C. Adeene Denton[1], Brandon C. Johnson[1,2], Shigeru Wakita[1], Andrew M. Freed[1], H. Jay Melosh[1,2,†], and S. Alan Stern[3]

[1]Department of Earth, Atmospheric, and Planetary Sciences, Purdue University, West Lafayette, IN, USA, [2]Department of Physics and Astronomy, Purdue University, West Lafayette, IN, USA, [3]Southwest Research Institute, Boulder, CO, USA

[†]Deceased 11th September 2020

Key Points:

- We model the formation of Pluto's Sputnik Planitia basin from an impact origin to assess the dwarf planet's interior structure
- Our simulations illustrate the Sputnik Planitia-forming impact is capable of producing significant antipodal terrains on Pluto
- The extent and mode of deformation at the antipode is most consistent with a thick (>150-km) ocean and a hydrated core

Supporting Information:

- Supporting Information S1
- Movie S1

Correspondence to:
C. A. Denton,
denton15@purdue.edu

Citation:
Denton, C. A., Johnson, B. C., Wakita, S., Freed, A. M., Melosh, H. J., & Stern, S. A. (2021). Pluto's antipodal terrains imply a thick subsurface ocean and hydrated core. *Geophysical Research Letters*, *48*, e2020GL091596. https://doi.org/10.1029/2020GL091596

Received 15 JUL 2020
Accepted 18 DEC 2020

Abstract Recent analysis of New Horizons data revealed an ~1,000-km-diameter region of large-scale lineations antipodal to Sputnik Planitia, the 1,200 × 2,000 km elliptical impact basin on Pluto's anti-Charon hemisphere. At the available resolution, these lineations are similar to antipodal terrains associated with large impact basins elsewhere in the Solar System. Here, we simulate the Sputnik Planitia-forming impact and track stress waves through a Pluto-like target body to the antipode. We find that the Sputnik Planitia-forming impact is capable of producing significant antipodal terrains and the observed lineations may be extensional graben. The extent and mode of deformation at the antipode, however, is sensitive to ocean thickness and core composition. Simulations that best reproduce the observed terrains imply that Pluto may have hosted a >150-km-thick ocean and a hydrated core at the time of impact.

Plain Language Summary Pluto's interior structure remains largely a mystery, including the composition of the core and the existence and extent of a subsurface ocean. Though seismological study is not yet possible on Pluto, the reaction of a planet's interior structure to stress waves produced by large impacts can be used to indirectly probe the planet's interior—seismology by impact. We use impact modeling to simulate the formation of Sputnik Planitia, Pluto's massive impact basin, to determine how the dwarf planet's interior controls transmission of stress waves to the opposite hemisphere. Our results suggest that a large subsurface ocean beneath the ice shell, as well as a core that has experienced substantial alteration from interactions with an ocean above, are critical to match the size of the lineated terrain observed antipodal to Sputnik Planitia.

1. Introduction

Large planetary impacts are believed to cause significant deformation on the opposite hemisphere of the target body as a consequence of focusing of the seismic waves produced from impact to the basin's antipode. Near-surface pressure gradients can produce significant deformation and surface disruption, resulting in antipodal terrains (Bowling et al., 2013; Hood & Artemieva, 2008; Schultz & Gault, 1975; Watts et al., 1991). The recently identified zone of lineations antipodal to Pluto's ancient Sputnik Planitia basin (Moore et al., 2016; Stern et al., 2020) superficially resemble antipodal terrains associated with the other largest impact basins in the Solar System, including the "hilly and lineated" terrain antipodal to Caloris Basin on Mercury (Schultz & Gault, 1975) and the disrupted terrain opposite the Imbrium basin on the Moon (Schultz & Gault, 1975). Pluto's lineations, however, are hundreds of km long and tens of kilometer wide, potentially much larger than any antipodal terrain observed elsewhere, though consistent with the large size of Sputnik Planitia relative to Pluto.

The low resolution of imagery of Pluto's far side (i.e., the hemisphere opposite Sputnik Planitia) limits further characterization of these features, including their topographic nature. However, their departure from trends in Pluto's large ridge-trough system and corresponding proximity to predicted potential antipodes of the Sputnik Planitia-forming impact suggest an impact origin is possible (Stern et al., 2020). Assuming these lineations are indeed antipodal features and not albedo markings produced otherwise (Stern et al., 2015), we explore their possible origin from the focusing of stress waves produced by the Sputnik Planitia impact.

The extent and mode of deformation experienced at the antipode to large impacts is directly related to variations in the bulk properties of the target body, which in turn affect how stress waves are focused and/or

dissipated. For rocky bodies, antipodal deformation is strongly dependent on sound speed, strength, and porosity contrasts between the mantle and core (Bowling et al., 2013; Watts et al., 1991); for ocean worlds, one expects both core composition and the added presence of a liquid layer in the interior will be dominant factors. Previous work concerning antipodal focusing on icy rather than rocky systems considered Saturn's mid-sized moons using a smooth particle hydrocode (Bruesch & Asphaug, 2004). However, this work was limited to ~10 km spatial resolution, much larger than the scale of most observed antipodal features, and did not incorporate the effects of a subsurface ocean on wave transmission. In this study, we model the Sputnik Planitia impact using a spatial resolution of 2 km, which is expected to resolve the extent, magnitude, and large-scale variations of strain at the antipode on the scale of the massive lineations observed, and consider variations in core composition and the presence/thickness of a subsurface ocean at the time of impact.

Here, we explore a range of impactor diameters, finding that a 400-km-diameter impactor traveling at 2 km/s best reproduces the updated dimensions of Sputnik Planitia (Schenk et al., 2018). We further explore a range of ice shell/ocean thickness parameters and core compositions to identify the interior structure of Pluto most consistent with an ~1,000-km-diameter region of antipodal deformation, which includes a 150-km-thick ocean and serpentine core, and illustrate how Pluto's internal structure dictates stress wave transmission to the antipode.

2. Materials and Methods

2.1. Impact Modeling

To determine whether the complex lineations approximately antipodal to Pluto's Sputnik Planitia may be causally related, we simulate the formation of Sputnik Planitia using the axisymmetric iSALE-2D shock physics code (Amsden et al., 1980; Collins et al., 2004; Wünnemann et al., 2006). Our axisymmetric models may enhance the degree of antipodal focusing. Although focusing in oblique impacts is more limited, significant damage is still expected for planetary-scale impacts (Schultz & Crawford, 2011; Stickle et al., 2015). While Sputnik Planitia's elliptical geometry suggests an oblique impact origin (e.g., Stern et al., 2020), the full implications of obliquity on concentrated antipodal deformation require full 3D models capable of tracking multiple materials, which is not currently possible with iSALE-3D. While two-dimensional simulations may not fully describe the complexity or style of deformation associated with oblique impacts, we consider them sufficient to characterize variations in antipodal deformation associated with changes in target material characteristics (ocean thickness and core composition), whose influence on stress wave transmission should remain consistent for both oblique and vertical impacts. Removal of the symmetry axis may reduce compressional focusing at the center of the antipodal zone, however. Antipodal deformation induced by oblique impacts is centered antipodal to the point of impact rather than the basin center, which is shifted downrange (Schultz & Crawford, 2011). Indeed, a possible offset in the antipodal terrain of Sputnik Planitia was noted by Stern et al. (2020).

The material parameters for the ice shell, ocean, and core are shown in Table S1. We model impacts of an icy body into a spherical, three-layer Pluto-like target with pressure- and temperature-dependent densities according to appropriate equations of state: we use the Tillotson equation of state for the impactor and the ice shell and the ANEOS equation of state for water for the subsurface ocean (Bray et al., 2014; Turtle & Pierazzo, 2001). We use the ANEOS equations of state for dunite or serpentine to represent Pluto's core (Benz et al., 1989; Brookshaw, 1998). Given the limited number of equations of state that accurately model the response of geologic materials to impact and the uncertainties in Pluto's formation history, we consider dunite and serpentine to be suitable materials to represent rocky (anhydrous, ordinary chondrites) and hydrous (carbonaceous chondrites) components in Pluto's core.

Ice shell strength and damage parameters come from fits to ice strength (Bray et al., 2014; Silber & Johnson, 2017). The core strength and thermal softening parameters come from fits to dunite rock strength (Davison et al., 2010; Potter et al., 2012). Following Johnson, Bowling, et al. (2016), we treat the ocean as a strengthless fluid. Thus, the effect of ocean temperature on our results is negligible. We incorporate a nonlinear thermal conductivity (Johnson et al., 2017), resulting in a temperature profile for a conducting shell given by

$$T(z) = T_s \left(\frac{T_b}{T_s} \right)^{\frac{z}{h_{\text{cond}}}} \quad (1)$$

where z is depth, T_s and T_b are the surface temperature and basal temperature, respectively, and h_{cond} is the assumed thickness of the conductive portion of the shell, which here represents the entire ice shell thickness (Table S2). We also utilize a full viscoelastic-plastic rheology for the ice shell to incorporate the viscous contribution to material strain (Elbeshausen & Melosh, 2020; Johnson, Bowling, et al., 2016). Inclusion of the viscoelastic-plastic rheology may affect final basin morphology, but will not influence transmission of stress waves or resulting antipodal deformation.

To assess the effect of ice shell/ocean thickness in addition to core composition, we produce simulations with four different preimpact ocean thicknesses of 0 (no ocean), 50, 100, and 150 km. To avoid any minor variations based on differences in preimpact thermal structures in the ice shell we hold the average thermal gradient in the ice shell at 0.8 K/km (Figure S1); we assume the ice shell is purely conductive. 0.8 K/km was selected as a stable thermal gradient for most ocean thicknesses following assessment of ice shell basal temperatures that permit stable liquid oceans, which can include colder ice shells than previously tested (Nimmo et al., 2016) if a thermal boundary layer is present at the ice shell/ocean interface (Kamata et al., 2019).

Table S3 describes the model setup used in all iSALE runs for this study. We apply the inferred mean impactor velocity for Pluto of ~2 km/s (Zahnle et al., 2003) and a realistic central gravity field that accounts for the effect of planetary curvature from the large size of the basin (Ivanov et al., 2010); testing at lower resolution shows that full self-gravity is not required (supporting information S1). Previous work also found that a dunite core radius of ~860 km reproduces the surface gravity of Pluto and is consistent with estimates of H_2O thickness and body radius (Johnson, Bowling, et al., 2016; Robuchon & Nimmo, 2011; Stern et al., 2015); as such, we hold constant both the radius of the core (860 km) and the combined thickness of the ice shell and ocean (328 km). Holding core size constant while varying core composition causes our simulated Pluto to be ~15%–16% less massive when a serpentine core is used; however, keeping ocean and ice shell thicknesses constant over all runs to directly assess how the ocean affects stress waves was considered more important than matching the mass of Pluto. The entirety of Pluto was simulated axisymmetrically at 2 km spatial resolution to resolve antipodal strains. Comparison with 1-km-resolution runs indicates that 2 km resolution is sufficient to characterize trends in deformation at the antipode (Figure S2).

Lastly, to reproduce the updated size estimates for Sputnik Planitia (Schenk et al., 2018), which are nearly double those used in previous impact simulations (Johnson, Bowling, et al., 2016), we also test a range of impactor diameters of 300, 350, 400, and 450 km to assess the effect of a much larger impactor on basin development (Figures S3 and S4). Crater scaling laws (Johnson, Collins, et al., 2016) suggest an updated impactor diameter close to 400 km using an estimated simple-to-complex transition of 6 km (Bray & Schenk, 2015). We find that a 400-km-diameter impactor produces a roughly 1600-km-diameter basin consistent with the average of the elliptical 1,200 × 2,000 km estimate of Schenk et al. (2018) (Figure S3). As such, we use a 400-km impactor for all subsequent runs in this study.

2.2. Strain Calculation

Determining which internal model produces adequate antipodal deformation requires quantifying which material regimes could induce faulting on the scale inferred by the observed lineations observed. Following impact modeling, we infer resulting deformation at the antipode through measurements of material velocity, displacement, and strain in the ice shell during and after stress wave arrival (Bowling et al., 2013). We determine the magnitude of strain experienced by material at the antipode during and after deformation as a proxy for estimates of fault initiation and magnitude. To calculate strain in the region surrounding the antipode, we analyzed the distance between adjacent massless tracer particles along a given depth for their initial positions at 0 s (when no antipodal deformation has taken place) and their resulting positions at ~5,000 s (when the antipode is no longer accumulating plastic strain and the majority of motion has ceased). In this scenario, negative strain is compressional (tracers moved closer together) and positive strain is extensional (tracers moved farther apart).

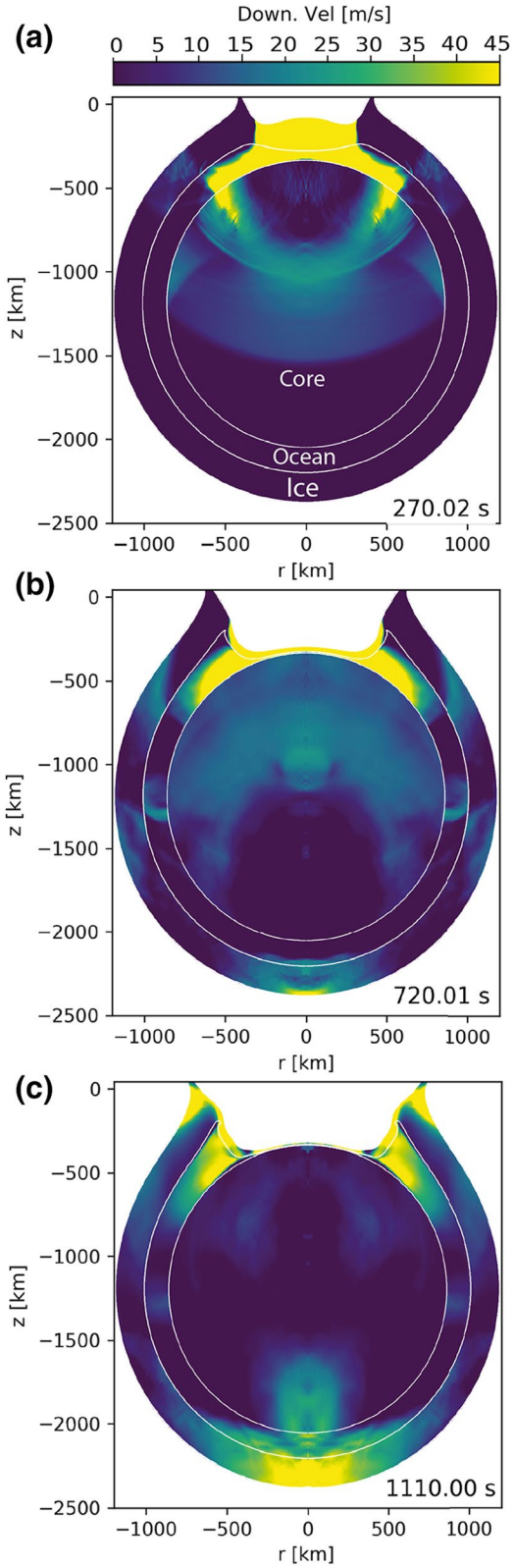

Figure 1. Propagation of impact stress wave and arrival at antipode. Cross-sections showing wave passage through Pluto's interior following impact of a 400-km-diameter impactor into a Pluto-like target with a 150-km-thick ocean (178-km-thick ice shell) and a serpentine core. Material colored according to magnitude of material velocity in the z-direction (downward), as indicated in the color bar. Collision site is at the origin. In (a) the wave is becoming temporally separated between materials (270 s into impact). Panel (b) shows arrival of the wave traveling through the core (720 s). Panel (c) illustrates wave arrival in the ice shell (1,110 s).

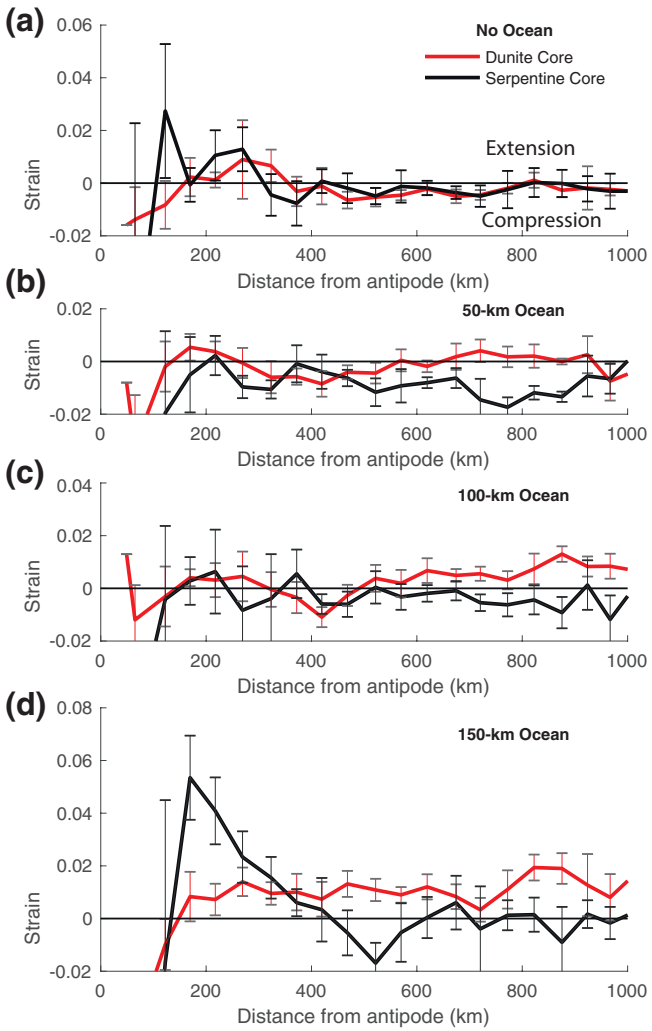

Figure 2. Strain component $\varepsilon_{\theta\theta}$ (unitless) near the antipode measured at 10 km depth and averaged in 50-km-wide bins for no ocean (a). A 50-km-thick ocean (278-km-thick ice shell) (b). A 100-km-thick ocean (228-km-thick ice shell) (c). A 150-km-thick ocean (178-km-thick ice shell) (d). For both dunite (red) and serpentine (black) cores. Error bars are 1 standard deviation from the mean. In some cases, strain near the antipode is compressive enough to be off the scale of the figure due to interaction with the symmetry axis.

We calculate strain according to the definitions of strain as applied to our axisymmetric model, which are given in target-centered in spherical (r, θ) coordinates following Slaughter (2012):

$$\varepsilon_{\theta\theta} = \frac{1}{r}\frac{\partial U_\theta}{\partial r} + \frac{U_r}{r} \quad (2)$$

$$\varepsilon_{\phi\phi} = \frac{U_\theta}{r}\cot\theta + \frac{U_r}{r} \quad (3)$$

Here $U_r = \delta r$ and $U_\theta = r\delta\theta$, representing distances of displacement. δr and $\delta\theta$ are differences between initial and final r (radius) and θ, respectively. The dominant mode of strain near the antipode is $\varepsilon_{\theta\theta}$, calculated along the curvature of Pluto in lines of constant longitude and shown in Figure 2. However, Pluto's ice shell also experiences strain across lines of constant latitude $\varepsilon_{\phi\phi}$; strain in $\varepsilon_{\theta\theta}$ and $\varepsilon_{\phi\phi}$ are compared in Figure S5. Although $\varepsilon_{\phi\phi}$ is compressional near the antipode, this compressional strain is overcome by $\varepsilon_{\theta\theta}$, which is larger in magnitude and extensional in the surrounding region. The definitions of both strain components also incorporate an element of radial deformation, which must be separated from the impact-induced oscillations of Pluto around its preimpact center (an effect produced by large impacts using central gravity). To correct our calculations of radial displacement we assume that the position of material ~1,000 km from the antipode remains unchanged postimpact; we use this point to calculate the target offset produced from oscillation (~4–6 km), which is used to correct postimpact positions across the body.

Tracer velocities, and thus the strain calculated from their resulting displacements, are subject to error. Tracer velocities in iSALE are determined by bilinear interpolation of the velocities in each cell of the grid; thus, when tracers move large distances during deformation (i.e., antipodal focusing), a small calculation error is introduced that may result in final positions that exceed or fall short of those expected. Strain calculations performed on these data inherit these errors, producing data with a broadly observable trend but considerable variation, with strain distributions around an observable mean (Figure S4). At Pluto's surface, tracer movement is unrestricted by overlying material and is subject to greater potential for error in strain calculations. To minimize this effect, we calculate strain using near-surface rather than surface estimates for tracer motion. After assessing trends in strain magnitude and extent at 5, 10, 20, and 50 km depth, we calculate strains at a depth of 10 km from the surface, shallow enough to adequately capture strain trends with distance from the antipode, but deep enough to reduce uncertainties induced from errors associated with tracer motion near a free surface.

3. Impact Modeling Results

Our models directly simulate the process of stress wave focusing at the antipode to Sputnik Planitia and illustrate how Pluto's internal structure dictates the magnitude and extent of stress wave arrival(s) at the antipode. As shown for the best fit case in Figure 1, the contrast in sound speeds between Pluto's water-ice shell (~3,300 m/s) and an assumed serpentine core (~5,300 m/s) causes the impact-induced stress wave to be transmitted quickly through the core (Figure 1b) and much more slowly through the overlying ice shell (Figure 1c). The temporal separation of the initially hemispherically expanding stress wave (Melosh, 1989) produces separate arrivals at the antipode, as observed in two strong peaks (>35 m/s) in downward material velocity (not to be confused with wave speed) at ~720 and ~1,110 s after impact (Figures 1b, 1c, and S6). The compressional wave in the ocean is further delayed, arriving ~1,550 s after impact. Wave propagation for all

simulations is qualitatively similar to the behavior observed in Figure 1, with slight variations in maximum velocities reached and time of arrival.

Internal ocean thickness has a strong effect on the extent and degree of antipodal deformation (Figure 2). For a stress wave encountering the boundary between high- and low-sound-speed materials, the amplitude of the transmitted wave depends on the acoustic impedance (the product of the sound speed and density) difference between the two materials (Melosh, 1989); a larger contrast in sound speed reduces wave transmission. The contrast in sound speeds between the core ($c_{\text{sepentine}} \approx 5{,}300$ m/s, $c_{\text{dunite}} \approx 6{,}500$ m/s) and the ocean ($c_{\text{ocean}} \approx 1{,}900$ m/s, Figure 2b) far exceeds that of the core and the ice shell ($c_{\text{ice}} \approx 3{,}300$ m/s). Additionally, shear waves are not transmitted through the strengthless ocean. Thus, inclusion of an ocean decreases transmission of stress waves through the core to the antipode, initially reducing deformation (Figures 2a and 2b). Transmission from the ice shell to the ocean is also inhibited; as such, when the ice shell is thin, energy and deformation are concentrated in the near-surface. This waveguide effect offsets the reduced transmission from the core for cases with a thick ocean and a thinner ice shell, resulting in larger antipodal deformation (Figure 2d).

Variations in core composition produce a separate trend in antipodal deformation: when a serpentine core ($c_{\text{sepentine}} \approx 5{,}300$ m/s) is used instead of dunite, ($c_{\text{dunite}} \approx 6{,}500$ m/s) the decrease in core sound speeds reduces the strong impedance contrast between Pluto's core and the overlying ocean, reducing stress wave reflection and increasing transmission. As such, overall energy transmission to the antipode is increased when the core is serpentinized through hydrothermal alteration (e.g., Figures 2a and 2d). In a scenario incorporating both a 150-km ocean and a serpentine core, enhanced ice shell transmission is accompanied by greater transmission of energy through the core, which combine to maximize deformation in the antipodal region (Figure 2d).

To determine the potential deformation experienced at the antipode to Sputnik Planitia, we infer structural responses based on the magnitude and regional extent of strains. The majority of the region surrounding the antipode undergoes extension, hence graben are expected. Horizontal displacement at the antipode for our best fit case occurs in a near-surface zone extending ~400–500 km from the antipode; this zone extends downward ~30–50 km from the surface and is characterized by ~4–14 km of transport inward toward the antipode. Expected strain near the antipode was calculated from tracer particle locations before and after impact at 10 km depth. The 100 km closest to the antipode sustains intense compression from the mass of material moved inwards by the stress wave, a reaction enhanced by proximity to the symmetry axis (Figure 2d). Farther beyond the symmetry axis lies a zone of elevated extensional strain as inferred by sustained strains of ~1%–3% (Figure 2d) that extends ~100–~500 km from the antipode. The radius of the model-estimated extension zone is consistent with the observed ~1,000-km zone of antipodal disruption (Figure 2d) and the tentative inference that the lineated features are depressions that may be structural in origin (Stern et al., 2020).

Topographic information is not available for Pluto's anti-Charon hemisphere where the antipodal terrains are observed (Schenk et al., 2018; Stern et al., 2020). However, if the lineations within the disrupted terrain are indeed associated with antipodal deformation from the formation of Sputnik Planitia, we expect them to be the remnants of a graben system produced from accommodation of the widespread extensional strains observed in our model results. Because strains are predominately extensional and $\varepsilon_{\theta\theta}$ exceeds $\varepsilon_{\phi\phi}$, we expect that the resulting graben will be circumferential with respect to the antipode (Mandl, 1988). Note, however that our axisymmetric model may favor extension in $\varepsilon_{\theta\theta}$. Furthermore, the inner 100 km zone of compression is likely to be topographically elevated.

Assuming that these lineations result from antipodal deformation, we can calculate likely graben depths produced from extensional strain at the antipode, assuming that average strain in the region is equally accommodated by formation of two to four graben (based on the observed distribution of lineations within the lineated terrain as mapped by Stern et al., 2020), and assuming that both bounding normal faults dip at $\theta = 60°$. Imagery for the antipodal region indicates a series of complex lineations, the discrete number of which varies depending on mapped interpretation; two to four graben were estimated as a benchmark for these features. To obtain accurate values for average strain accommodated by these potential graben, we took the average of the strain values measured in the extensional zone, which was then defined as the

average strain for the entirety of the antipodal region. Strains in the small compression zone near the symmetry axis were excluded.

From this formulation, we determine that the resulting graben may be between 4.4 and 2.2 km deep (for two and four graben, respectively), similar in scale to the massive graben measured in Viking Terra and Cthulhu Regio on Pluto's nearside (Conrad et al., 2019; Schenk et al., 2018). Current image resolution cannot confirm or rule out the presence of additional smaller graben families surrounding these features, which could contribute to accommodation of regional strain; however, the larger main graben are expected to accommodate the majority of the strain.

All of our simulations produce some amount of surficial deformation at the antipode based on the resulting elevated strains (Figure 2); however, only our best-fitting simulation is consistent with both the magnitude and lateral extent (~500 km radius) of strain required to produce the lineated features. Scenarios involving dunite cores and thinner oceans produce weaker zones of extensional strain focused closer to the antipode (Figures 2a–2c). Utilizing the same formulation for strain allocation as above, accounting for differences in radial extent of the extension zone, indicates that graben of a similar size (~1.6–2.7 km depth) may form for a serpentine core without an ocean. This depth is further reduced to ~0.5–1.1 km for a dunite case; however, in both scenarios, the overall zone of extension falls short by ~100–200 km of the extent of the lineations observed. For both 50- and 100-km-thick oceans, low average strains imply any potential graben might be less than 300 m deep. All alternate models fail to produce deformation over a sufficient extent from the antipode, with one exception: when a 150-km-thick ocean is paired with a dunite core, the waveguide effect in the ice shell produces ~0.5% extensional strains extending far from the antipode (Figure 2). However, resulting graben at these low strains are expected to be between 360 and 540 m deep, distributed over a much larger extension zone ~1,000 km in radius, inconsistent with the magnitude and extent of the lineations observed.

4. Implications for Pluto's Interior

Our best-fit simulations suggest that significant water/rock interaction must occur in Pluto's interior prior to the formation of Sputnik Planitia to produce the serpentine core required to produce the observed lineations in an antipodal deformation scenario. Partial or complete serpentinization of the core is feasible for temperatures reached during Pluto's early evolution (Wakita & Sekiya, 2011) depending on the timescale of Pluto's initial formation and differentiation in the early Solar System. As serpentinization is an exothermic reaction, runaway serpentinization may occur associated with higher temperatures produced by ^{26}Al decay for the first few Myr after Solar System formation (Wakita & Sekiya, 2011), provided that circulation of warm water throughout large portions of the core is a possibility. However, full serpentinization of the core is not necessarily required; the impedance contrast produced by a partially hydrated core could yield similarly efficient energy transmission between the core and overlying ocean, provided that the transition between nonhydrated (dunite) to hydrated (serpentine) materials is relatively smooth and the hydrated region is comparable in scale to the width of the stress wave. From such estimates we predict an ~75–125 km zone of hydration extending downward from the core-ocean interface, a remnant of significant hydrothermal alteration on early Pluto. Overall, our analysis suggests that Pluto possesses a serpentine core, a possibility previously suggested by some models of Pluto's thermal evolution (Bierson et al., 2018; Robuchon & Nimmo, 2011). Due to the dependence of wave focusing on sound speed rather than strictly composition, we note that a core composition with similar material strength and sound speed to serpentine would result in similar antipodal deformation to that observed in our best-fit case. However, when considering our results in the context of previous thermal modeling (Bierson et al., 2018; Robuchon & Nimmo, 2011), we consider the presence of a serpentine core to be a robust possibility.

In addition to our predictions for core composition, our simulations also suggest a thick ocean is required to reproduce the extent of Pluto's observed antipodal terrain regardless of core composition (Figure 2d). The presence of an ocean has been suggested from several lines of geologic evidence, including widespread extensional tectonics (Hammond et al., 2016), the absence of a fossil bulge (Stern et al., 2018), and the location of Sputnik Planitia near the Pluto-Charon tidal axis (Keane et al., 2016; Nimmo et al., 2016). Our analysis presents another independent piece of evidence in its favor. The presence of potential impurities in

Pluto's ocean, particularly salt and ammonia, is likely, though in relatively low concentrations (e.g., Kamata et al., 2019). These impurities may improve stress wave transmission through the ocean, as increased salinity is correlated with a minor increase in sound speed (Wong & Zhu, 1995). However, the sound speed increase from increased salinity (~300–400 m/s, Wong & Zhu, 1995) is relatively minor in comparison to the contrast between the core and ocean, which is ~3,400 m/s for the serpentine core. While our formulation of the ice shell for these tests assumes a fully conductive shell, the presence of convective ice at the time of Sputnik Planitia's formation is possible (Robuchon & Nimmo, 2011). However, the sound speed for convecting versus nonconvecting ice under identical pressure conditions varies by ~0.1% in our models, and thus convection does not present a significant control on antipodal deformation.

Topographic information remains unavailable to assess whether these features are indeed tectonic in origin or simply albedo features (Stern et al., 2020); however, if these features are indeed of a tectonic and impact origin, their current approximate (~1,000 km) extent is most consistent with deformation maximized by a substantial ocean and a potentially hydrated core. Although the formation process of large Kuiper Belt objects is still debated (e.g., Kenyon et al., 2008; Morbidelli & Nesvorný, 2020), they may have similar compositions. Given the general thermal evolution of surrounding icy planetesimals in the early solar nebula (Wakita & Sekiya, 2011), other Kuiper Belt dwarf planets of a similar size and formation age may have experienced similar complex interior histories.

5. Conclusions

We have conducted an analysis of the effects of internal structural and compositional variations on antipodal focusing from the Sputnik Planitia impact to determine whether the lineations observed could feasibly have an impact origin. We find that the Sputnik Planitia-forming impact was likely associated with a 400-km-diameter impactor at a speed of 2 km/s and is indeed capable of producing significant antipodal terrains on Pluto. Our models suggest that, for an impact origin, the extent of the lineations observed is most consistent with antipodal deformation associated with a 150-km-thick ocean and a hydrated core at the time of Sputnik Planitia's formation. These results further support the presence of a subsurface ocean as well as significant water-rock interactions in Pluto's interior.

Data Availability Statement

At present, iSALE is not fully open source. It is distributed on a case-by-case basis to academic users in the impact community, strictly for noncommercial use. Scientists interested in using or developing iSALE should see http://www.isale-code.de/redmine/projects/isale/wiki/Terms_of_use for a description of application requirements. Model output has been published at the Harvard Dataverse, https://doi.org/10.7910/DVN/IU7185.

Acknowledgments
We gratefully acknowledge the developers of iSALE, including Gareth Collins, Kai Wünnemann, Dirk Elbeshausen, Tom Davison, and Boris Ivanov. Some plots in this study were created with the pySALEPlot tool written by Tom Davison. We also thank Francis Nimmo for fruitful discussions. C. Adeene Denton was supported by a NASA Future Investigators in Earth and Space Sciences and Technology award. S. Alan Stern was supported by the NASA New Horizons project for his contributions.

References

Amsden, A. A., Ruppel, H. M., & Hirt, C. W. (1980). *SALE: A simplified ALE computer program for fluid flow at all speeds*. Los Alamos, NM: Los Alamos Scientific Lab. https://doi.org/10.2172/5176006

Benz, W., Cameron, A. G. W., & Melosh, H. J. (1989). The origin of the Moon and the single-impact hypothesis III. *Icarus*, *81*(1), 113–131. https://doi.org/10.1016/0019-1035(89)90129-2

Bierson, C. J., Nimmo, F., & McKinnon, W. B. (2018). Implications of the observed Pluto–Charon density contrast. *Icarus*, *309*, 207–219. https://doi.org/10.1016/j.icarus.2018.03.007

Bowling, T. J., Johnson, B. C., Melosh, H. J., Ivanov, B. A., O'Brien, D. P., Gaskell, R., & Marchi, S. (2013). Antipodal terrains created by the Rheasilvia basin forming impact on asteroid 4 Vesta. *Journal of Geophysical Research: Planets*, *118*(9), 1821–1834. https://doi.org/10.1002/JGRE.20123@10.1002/(ISSN)2169-9100.VESTAS1

Bray, V. J., Collins, G. S., Morgan, J. V., Melosh, H. J., & Schenk, P. M. (2014). Hydrocode simulation of Ganymede and Europa cratering trends - how thick is Europa's crust? *Icarus*, *231*, 394–406. https://doi.org/10.1016/j.icarus.2013.12.009

Bray, V. J., & Schenk, P. M. (2015). Pristine impact crater morphology on Pluto - Expectations for New Horizons. *Icarus*, *246*, 156–164 https://doi.org/10.1016/j.icarus.2014.05.005

Brookshaw, L. (1998). *Working paper series SC-MC-9813*. Australia: Faculty of Sciences, University Southern Queensland.

Bruesch, L. S., & Asphaug, E. (2004). Modeling global impact effects on middle-sized icy bodies: Applications to Saturn's moons. *Icarus*, *168*(2), 457–466 https://doi.org/10.1016/j.icarus.2003.11.007

Collins, G. S., Melosh, H. J., & Ivanov, B. A. (2004). Modeling damage and deformation in impact simulations. *Meteoritics & Planetary Science*, *39*(2), 217–231. https://doi.org/10.1111/j.1945-5100.2004.tb00337.x

Conrad, J. W., Nimmo, F., Schenk, P. M., McKinnon, W. B., Moore, J. M., Beddingfield, C. B., et al. (2019). An upper bound on Pluto's heat flux from a lack of flexural response of its normal faults. *Icarus*, *328*, 210–217. https://doi.org/10.1016/j.icarus.2019.03.028

Davison, T. M., Collins, G. S., & Ciesla, F. J. (2010). Numerical modelling of heating in porous planetesimal collisions. *Icarus*, *208*(1), 468–481. https://doi.org/10.1016/j.icarus.2010.01.034
Elbeshausen, D., & Melosh, J. (2020). A nonlinear and time-dependent visco-elasto-plastic rheology model for studying shock-physics phenomena. *Engineering Reports*, e12322. https://doi.org/10.1002/eng2.12322
Hammond, N. P., Barr, A. C., & Parmentier, E. M. (2016). Recent tectonic activity on Pluto driven by phase changes in the ice shell. *Geophysical Research Letters*, *43*, 6775–6782. https://doi.org/10.1002/2016GL069220
Hood, L. L., & Artemieva, N. A. (2008). Antipodal effects of lunar basin-forming impacts: Initial 3D simulations and comparisons with observations. *Icarus*, *193*(2), 485–502. https://doi.org/10.1016/j.icarus.2007.08.023
Ivanov, B., Melosh, H., & Pierazzo, E. (2010). Basin-forming impacts: Reconnaissance modeling. *America Special Paper*, *465*, 29–49. https://doi.org/10.1130/2010.2465(03)
Johnson, B. C., Bowling, T. J., Trowbridge, A. J., & Freed, A. M. (2016). Formation of the Sputnik Planum basin and the thickness of Pluto's subsurface ocean. *Geophysical Research Letters*, *43*, 10068–10077. https://doi.org/10.1002/2016GL070694
Johnson, B. C., Collins, G. S., Minton, D. A., Bowling, T. J., Simonson, B. M., & Zuber, M. T. (2016). Spherule layers, crater scaling laws, and the population of ancient terrestrial impactors. *Icarus*, *271*, 350–359. https://doi.org/10.1016/j.icarus.2016.02.023
Johnson, B. C., Sheppard, R. Y., Pascuzzo, A. C., Fisher, E. A., & Wiggins, S. E. (2017). Porosity and Salt Content Determine if Subduction Can Occur in Europa's Ice Shell. *Journal of Geophysical Research: Planets*, *122*(12), 2765–2778. https://doi.org/10.1002/2017JE005370
Kamata, S., Nimmo, F., Sekine, Y., Kuramoto, K., Noguchi, N., Kimura, J., & Tani, A. (2019). Pluto's ocean is capped and insulated by gas hydrates. *Nature Geoscience*, *12*, 407–410. https://doi.org/10.1038/s41561-019-0369-8
Keane, J. T., Matsuyama, I., Kamata, S., & Steckloff, J. K. (2016). Reorientation and faulting of Pluto due to volatile loading within Sputnik Planitia. *Nature*, *540*, 90–93. https://doi.org/10.1038/nature20120
Kenyon, S. J., Bromley, B. C., O'brien, D. P., & Davis, D. R. (2008). Formation and collisional evolution of Kuiper Belt objects. In M. A. Barucci (Ed.), *The solar system beyond Neptune*, (293–314). Tucson: University of Arizona Press.
Mandl, G. (1988). *Mechanics of tectonic faulting*. Amsterdam: Elsevier.
Melosh, H. J. (1989). *Impact cratering: A geologic process*. New York, NY: Oxford University Press.
Moore, J. M., McKinnon, W. B., Spencer, J. R., Howard, A. D., Schenk, P. M., Beyer, R. A., et al. (2016). The geology of Pluto and Charon through the eyes of New Horizons. *Science*, *351*(6279), 1284–1293. https://doi.org/10.1126/science.aad7055
Morbidelli, A., & Nesvorný, D. (2020). Kuiper belt: Formation and evolution. In D. Prialnik M. A. Barucci & L. Young (Eds.), *The trans-neptunian solar system* (pp. 25–59). Elsevier. https://doi.org/10.1016/b978-0-12-816490-7.00002-3
Nimmo, F., Hamilton, D. P., Mckinnon, W. B., Schenk, P. M., Binzel, R. P., Bierson, C. J., et al. (2016). Reorientation of Sputnik Planitia implies a subsurface ocean on Pluto. *Nature*, *540*, 7631. https://doi.org/10.1038/nature20148
Potter, R. W. K., Collins, G. S., Kiefer, W. S., McGovern, P. J., & Kring, D. A. (2012). Constraining the size of the South Pole-Aitken basin impact. *Icarus*, *220*(2), 730–743. https://doi.org/10.1016/j.icarus.2012.05.032
Robuchon, G., & Nimmo, F. (2011). Thermal evolution of Pluto and implications for surface tectonics and a subsurface ocean. *Icarus*, *216*(2), 426–439. https://doi.org/10.1016/j.icarus.2011.08.015
Schenk, P. M., Beyer, R. A., McKinnon, W. B., Moore, J. M., Spencer, J. R., White, O. L., et al. (2018). Basins, fractures and volcanoes: Global cartography and topography of Pluto from New Horizons. *Icarus*, *314*, 400–433. https://doi.org/10.1016/J.ICARUS.2018.06.008
Schultz, P. H., & Crawford, D. A. (2011). Origin of nearside structural and geochemical anomalies on the Moon. *Geological Society of America Special Paper*, *477*, 141–159. https://doi.org/10.1130/2011.2477(07)
Schultz, P. H., & Gault, D. E. (1975). Seismic effects from major basin formations on the moon and mercury. *The Moon*, *12*(2), 159–177. https://doi.org/10.1007/BF00577875
Silber, E. A., & Johnson, B. C. (2017). Impact Crater Morphology and the Structure of Europa's Ice Shell. *Journal of Geophysical Research: Planets*, *122*(12), 2685–2701. https://doi.org/10.1002/2017JE005456
Slaughter, W. S. (2012). *The linearized theory of elasticity*. Boston, MA: Springer Science & Business Media.
Stern, S. A., Bagenal, F., Ennico, K., Gladstone, G. R., Grundy, W. M., McKinnon, W. B., et al. (2015). The Pluto system: Initial results from its exploration by New Horizons. *Science*, *350*(6258), aad1815. https://doi.org/10.1126/science.aad1815
Stern, S. A., Grundy, W. M., Mckinnon, W. B., Weaver, H. A., & Young, L. A. (2018). The Pluto system after new horizons. *Annual Review of Astronomy and Astrophysics*, *56*, 357–392. https://doi.org/10.1146/annurev-astro-081817
Stern, S. A., White, O. L., McGovern, P. J., Keane, J. T., Conrad, J. W., Bierson, C. J., et al. (2020). Pluto's far side. *Icarus*, *356*, 113805. https://doi.org/10.1016/j.icarus.2020.113805
Stickle, A. M., Schultz, P. H., & Crawford, D. A. (2015). Subsurface failure in spherical bodies: A formation scenario for linear troughs on Vesta's surface. *Icarus*, *247*, 18–34. https://doi.org/10.1016/j.icarus.2014.10.002
Turtle, E. P., & Pierazzo, E. (2001). Thickness of a European ice shell from impact crater simulations. *Science*, *294*(5545), 1326–1328. https://doi.org/10.1126/science.1062492
Wakita, S., & Sekiya, M. (2011). Thermal evolution of icy planetesimals in the solar nebula. *Earth Planets and Space*, *63*(12), 1193–1206. https://doi.org/10.5047/eps.2011.08.012
Watts, A. W., Greeley, R., & Melosh, H. J. (1991). The formation of terrains antipodal to major impacts. *Icarus*, *93*(1), 159–168. https://doi.org/10.1016/0019-1035(91)90170-X
Wong, G., & Zhu, S. (1995). Speed of sound in seawater as a function of salinity, temperature, and pressure. *The Journal of the Acoustical Society of America*, *97*, 1732. https://doi.org/10.1121/1.413048
Wünnemann, K., Collins, G. S., & Melosh, H. J. (2006). A strain-based porosity model for use in hydrocode simulations of impacts and implications for transient crater growth in porous targets. *Icarus*, *180*(2), 514–527. https://doi.org/10.1016/j.icarus.2005.10.013
Zahnle, K., Schenk, P., Levison, H., & Dones, L. (2003). Cratering rates in the outer solar system. *Icarus*, *163*(2), 263–289. https://doi.org/10.1016/S0019-1035(03)00048-4

References From the Supporting Information

Bierson, C. J., Nimmo, F., & Stern, S. A. (2020). Evidence for a hot start and early ocean formation on Pluto. *Nature Geoscience*, *13*(7), 468–472. https://doi.org/10.1038/s41561-020-0595-0
Boadu, F. K. (2000). Wave propagation in fluid-saturated media: Waveform and spectral analysis. *Geophysical Journal International*, *141*(1), 227–240. https://doi.org/10.1046/j.1365-246X.2000.00073.x

Gabasova, L., Tobie, G., & Choblet, G. (2018). Compaction-driven evolution of Pluto's rocky core: Implications for water-rock interactions. *Ocean Worlds 2018*, Houston, TX: Lunar and Planetary Institute.

McKinnon, W. B., Stern, S. A., Weaver, H. A., Nimmo, F., Bierson, C. J., Grundy, W. M., et al. (2017). Origin of the Pluto–Charon system: Constraints from the New Horizons flyby. *Icarus*, *287*, 2–11. https://doi.org/10.1016/j.icarus.2016.11.019

Nur, A., & Simmons, G. (1969). The effect of saturation on velocity in low porosity rocks. *Earth and Planetary Science Letters*, *7*(2), 183–193. https://doi.org/10.1016/0012-821X(69)90035-1

Ogushwitz, P. R. (1985). Applicability of the Biot theory. I. Low-porosity materials. *The Journal of the Acoustical Society of America*, *77*(2), 429. https://doi.org/10.1121/1.391863

Pierazzo, E., & Melosh, H. J. (2000). Understanding oblique impacts from experiments, observations, and modeling. *Annual Review of Earth and Planetary Sciences*, *28*(1), 141–167.

Toksöz, M. N., Cheng, C. H., & Timur, A. (1976). Velocities of seismic waves in porous rocks. *Geophysics*, *41*(4), 621–645 https://doi.org/10.1190/1.1440639

Wyllie, M. R. J., Gregory, A. R., & Gardner, L. W. (1956). Elastic wave velocities in heterogeneous and porous media. *Geophysics*, *21*(1), 41–70. https://doi.org/10.1190/1.1438217